Injectable photosensitive bone cement enhancing angiogenesis and osteogenic differentiation for the treatment of bone nonunion

Cite as: APL Bioeng. **9**, 016114 (2025); doi: 10.1063/5.0246207
Submitted: 31 October 2024 · Accepted: 22 February 2025 ·
Published Online: 11 March 2025

View Online Export Citation CrossMark

Mengnan Wen,[1] Xueqiang Guo,[1] Yan Gong,[2] Fei Xue,[1] Zhenlin Fan,[1] Zhanting Kang,[3] Jixiang Li,[4] Lei Wang,[1,a)] Xiansong Wang,[1,2,a)] and Wenjie Ren[1,a)]

AFFILIATIONS

[1]Institutes of Health Central Plain, The Third Affiliated Hospital of Xinxiang Medical University, Clinical Medical Center of Tissue Engineering and Regeneration, Xinxiang Medical University, Xinxiang 453003, People's Republic of China
[2]Shanghai Key Laboratory of Tissue Engineering, Shanghai Ninth People's Hospital, Shanghai Jiao Tong University School of Medicine, Shanghai 200011, People's Republic of China
[3]Department of Pathology, School of Basic Medical Science, Xinxiang Medical University, Xinxiang 453003, People's Republic of China
[4]Junji College of Xinxiang Medical University, Xinxiang Medical University, Xinxiang 453003, People's Republic of China

[a)]**Authors to whom correspondence should be addressed:** lwang0522@163.com; wonderluis@sjtu.edu.cn; and wjren1966@163.com

ABSTRACT

Nonunion fractures present a significant clinical challenge because of their complex microenvironment, which includes poor vascularization, insufficient osteogenesis, infection, and separation of fracture ends. The current clinical treatments have certain limitations. Inspired by this phenomenon, sandcastle worms secrete adhesive proteins that bind sand grains, shell fragments, and mineral particles, thereby constructing their "castles." In this study, we developed an injectable bone cement using methacryloyl chitosan (CSMA) combined with a specific concentration of oyster shell nanoparticles (OS-np) to treat nonunion fractures. Oyster shells are composed primarily of calcium carbonate, which releases ions that promote angiogenesis and osteogenesis. The *in vivo* results at 8 weeks showed that the expression of BMP2, RUNX2, and VEGF in the OS-np/CSMA group was increased by 5.47, 4.38, and 3.54 times, respectively, compared to the control group, significantly enhancing vascularization and bone repair in the bone nonunion model. The injectability of the OS-np/CSMA bone cement ensures that it can adapt well to the complex structures of nonunion sites, providing a supportive matrix for new bone formation. Both *in vivo* and *in vitro* osteogenesis experiments demonstrated that the OS-np/CSMA bone cement significantly enhanced vascularization and bone repair in nonunion models, which was because of the synergistic effects of ion release and the bioactive properties of the oyster shell nanoparticles. This study highlights the potential of OS-np/CSMA injectable bone cement as a promising treatment strategy for complex nonunion fractures that effectively promotes angiogenesis and osteogenesis.

I. INTRODUCTION

Critical bone defects are common orthopedic conditions, typically resulting from trauma, tumors, congenital disorders, or degenerative diseases.[1] Commonly used clinical treatments include autografting, allografting, and bone graft substitutes.[2] However, their application is limited by donor shortage, weak osteoinductive capacity, susceptibility to infection, and high costs. Autologous bone, known for its excellent ability to promote bone formation and blood vessel growth, has traditionally been regarded as the "gold standard" in the clinical treatment of severe bone defects.[3] Nonetheless, it has limitations such as donor scarcity, high morbidity at the donor site, and significant surgical risks. In contrast, allogeneic bone undergoes immune rejection.[4]

Bone cement is widely used in orthopedic surgery to provide immediate mechanical stability for fractures and bone defects, facilitating early weight-bearing and functional recovery.[5] Additionally, it can be loaded with antibiotics to aid in infection control and prevention, making it particularly valuable for managing complex bone defects.[6,7]

However, traditional bone cement lacks osteoconductive and osteoinductive properties, and its mechanical performance is often inadequate to satisfy the mechanical strength required for long-term bone regeneration.[8] Moreover, despite their good mechanical strength and biocompatibility, some bone cements release a significant amount of heat during the curing process.[9] A new bone cement that meets the microenvironmental conditions for bone regeneration is urgently needed.[10]

Chitosan (CS), a natural polysaccharide derived from shellfish,[11] is widely used in tissue regeneration scaffolds due to its outstanding biocompatibility, biodegradability, biosafety, antibacterial properties, and ability to reduce inflammation.[12] Methacryloyl chitosan (CSMA) is produced by introducing methacrylate groups into the chitosan molecular chain, thereby endowing it with photocuring capabilities and mechanical strength.[13] Additionally, previous studies have shown that CSMA possesses antibacterial properties, reduces the risk of postoperative infection, enhances drug stability, controls drug release rates, and improves drug bioavailability.[14] Through photopolymerization, the CSMA forms a stable gel structure *in vivo*, providing a supportive environment. Nonetheless, the standalone "cement" does not provide sufficient mechanical support and often requires "sand" for reinforcement.

CSMA is the cement in the concrete, and here, a kind of sand is still missing. Oyster shells are a natural biomaterial. OS-np is obtained by grinding and screening fresh oyster shells and is rich in Ca^{2+}, Mg^{2+}, Sr^{2+}, and Si^{4+}, all of which are beneficial for bone repair and angiogenesis.[15,16] Studies have shown that these ions play a crucial role in bone formation, not only by promoting bone synthesis but also by enhancing the mechanical strength of new bone tissue.[17,18] OS-np has been reported to possess osteoinductive and osteoconductive capabilities, and its porous structure promotes cell adhesion and proliferation.[19,20] However, OS degrades slowly and has limited absorption.[21] Despite these limitations, OS is a cost-effective and readily available natural resource, which makes it feasible for large-scale clinical applications.

In nature, the glue secreted by sandcastle worms can bind sand grains, shell fragments, and other small particles together to construct "castles."[22] This glue exhibits excellent bonding properties, and the sandcastle habitat formed after curing exhibits superior structural stability and waterproofing characteristics. In bone-defect environments, the filling biomaterials must possess outstanding structural stability and remain stable in the presence of blood. Inspired by this phenomenon, we have developed a novel type of bone cement. We used chitosan-based hydrogel (CSMA), derived from natural marine organisms, to mimic the sandcastle worm glue; oyster shell nanoparticles, which release multiple pro-angiogenic and osteoinductive factors and provide a calcium source, were used to simulate the sand. The combination of these two materials results in bone cement with excellent curing properties, improved mechanical strength, and good osteoinductive properties. The synergistic effect of the CSMA and OS creates a bone-cement material that possesses mechanical strength, outstanding bioactivity, and regenerative potential. Consequently, we developed a new bone-cement material (Fig. 1).

II. RESULTS AND DISCUSSION

A. Preparation and characterization of OS-np

To obtain OS-np, fresh oyster shells [Fig. 2(a)] were ground into nanoparticles [Fig. 2(b)]. The ground material was sieved to select fine OS nanoparticles, which were then imaged using a scanning electron microscope (SEM) [Figs 2(c) and 2(d)]. Figure 2(c) presents the SEM image of OS-np at a lower magnification with a scale bar of 5 μm,

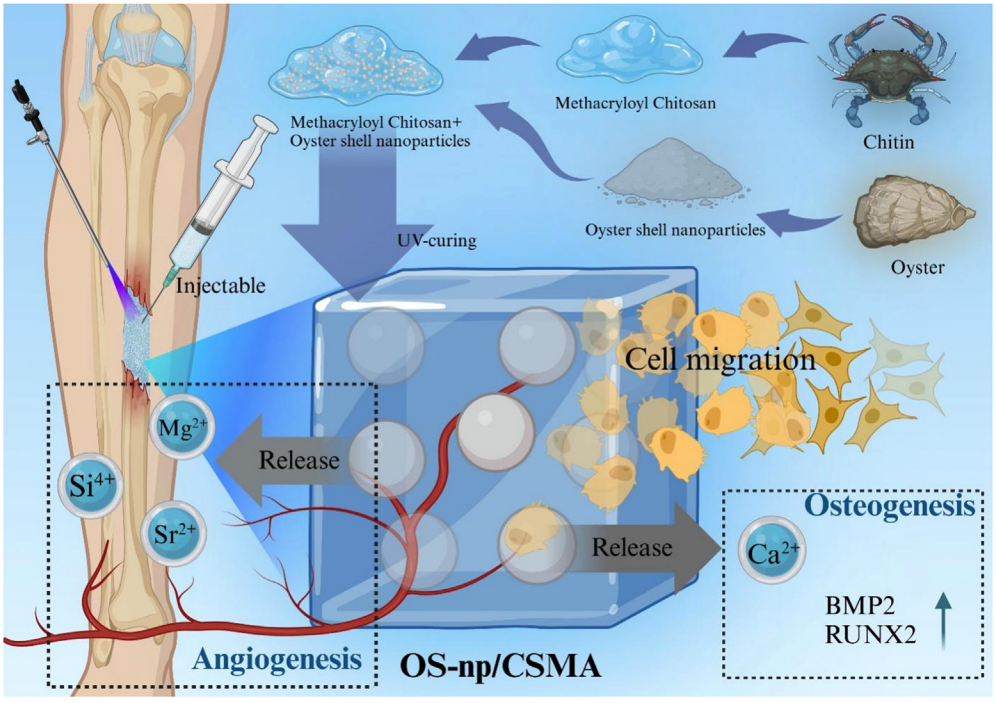

FIG. 1. Schematic diagram of the OS-np/CSMA interaction.

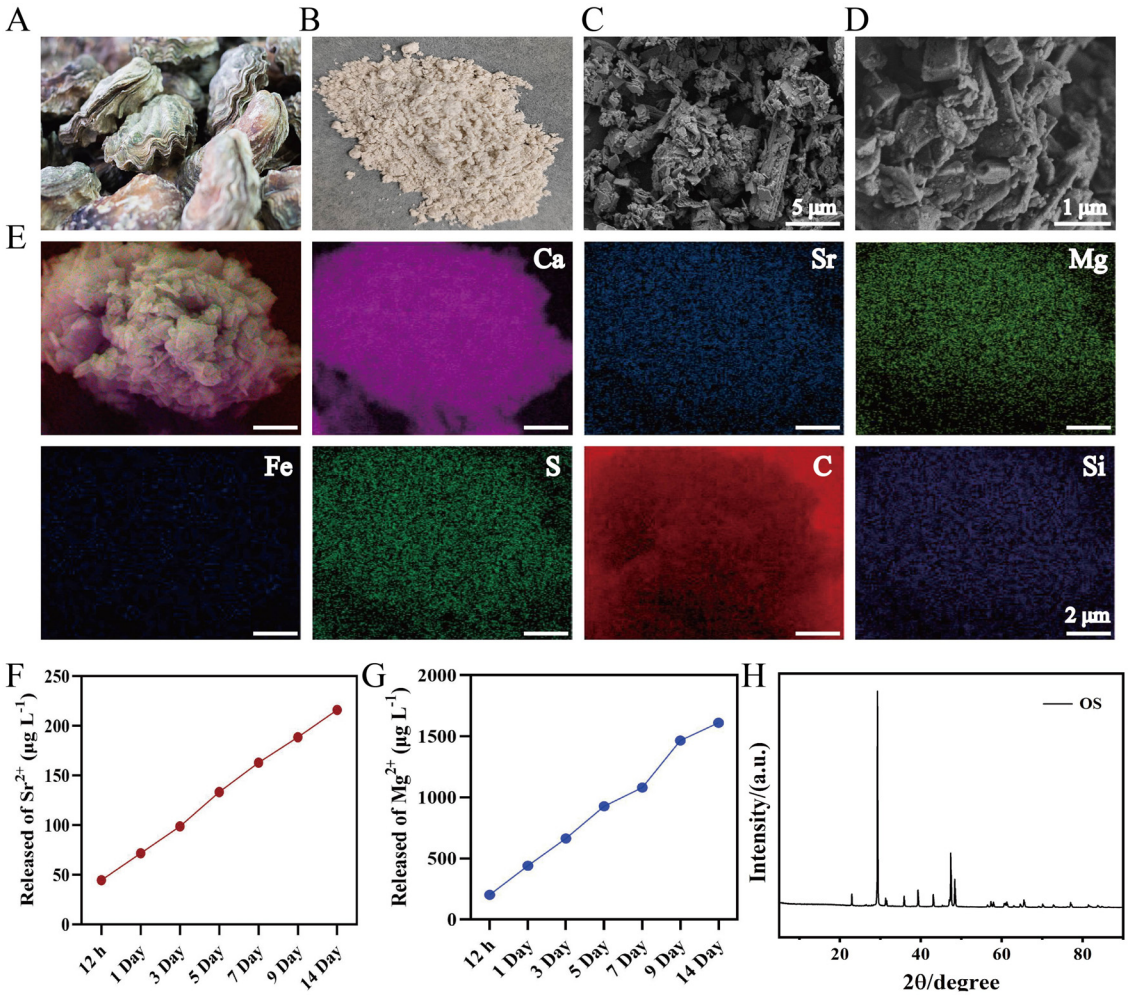

FIG. 2. Characterization of OS-np. (a) Appearance and morphology of OS-np. (b) OS nanoparticles. (c) SEM image of OS-np. Scale bar = 5 μm (d) SEM image of OS-np. Scale bar = 1 μm. (e) EDS element mapping of OS-np, showing all the elements contained in OS-np. (f) Concentration of magnesium ions (Mg^{2+}) released from OS-np at various times (12 h, 1 day, 3 days, 5 days, 7 days, 9 days, and 14 days). (g) Concentration of strontium ions (Sr^{2+}) released from OS-np at various times (12 h, 1 day, 3 days, 5 days, 7 days, 9 days, and 14 days). (h) XRD pattern of OS-np.

while Fig. 2(d) is a magnified view of Fig. 2(c) with a scale bar of 1 μm. The higher magnification image in Fig. 2(d) provides a clearer view of the OS-np morphology, indicating that the OS-np particles were relatively uniform. Energy-dispersive x-ray spectroscopy (EDS) revealed the uniform distribution of Ca, Sr, Mg, Fe, S, C, and Si in OS-np [Fig. 2(e)]. Fourier transform infrared spectroscopy (FT-IR) illustrates the correct structure of OS-np (Fig. 2, supplementary material). To verify ion release from OS-np, inductively coupled plasma optical emission spectrometry (ICP-OES) was employed to examine the OS-np aqueous solution. The results showed that the OS-np continuously released Mg^{2+} and Sr^{2+} [Figs. 2(f) and 2(g)]. OS-np was further examined by x-ray diffraction (XRD) [Fig. 2(h)]. The nanoribbons displayed distinct Bragg reflections, indicating high crystallinity. The XRD pattern of the nanoribbons revealed strong peaks at 29.3°, corresponding to OS-np. The results demonstrated that OS contains multiple bone-promoting ions and can provide a calcium source, making it a good bioactive factor.

B. Synthesis and characterization of OS-np/CSMA bone cement

Because CSMA has excellent biocompatibility and biodegradability and can enhance drug stability, control release rates, and improve bioavailability, it is widely used in the medical, pharmaceutical, and environmental fields.[17] It possesses injectability (Fig. 1, supplementary material). However, its mechanical strength was insufficient for bone regeneration, whereas OS-np exhibited good mechanical properties. We hypothesized that the addition of OS-np would improve the structural stability of the CSMA.[23] To obtain the optimal OS-np/CSMA ratio, we synthesized OS-np/CSMA bone cement with different concentrations of the OS-np solution [Fig. 3(a)]. Visually, it can be observed that as the OS-np solution is added, the color of CSMA gradually changes from transparent to milky white, and the higher the OS-np concentration, the more pronounced the color becomes. In bone regeneration, tissue engineering materials need to provide appropriate

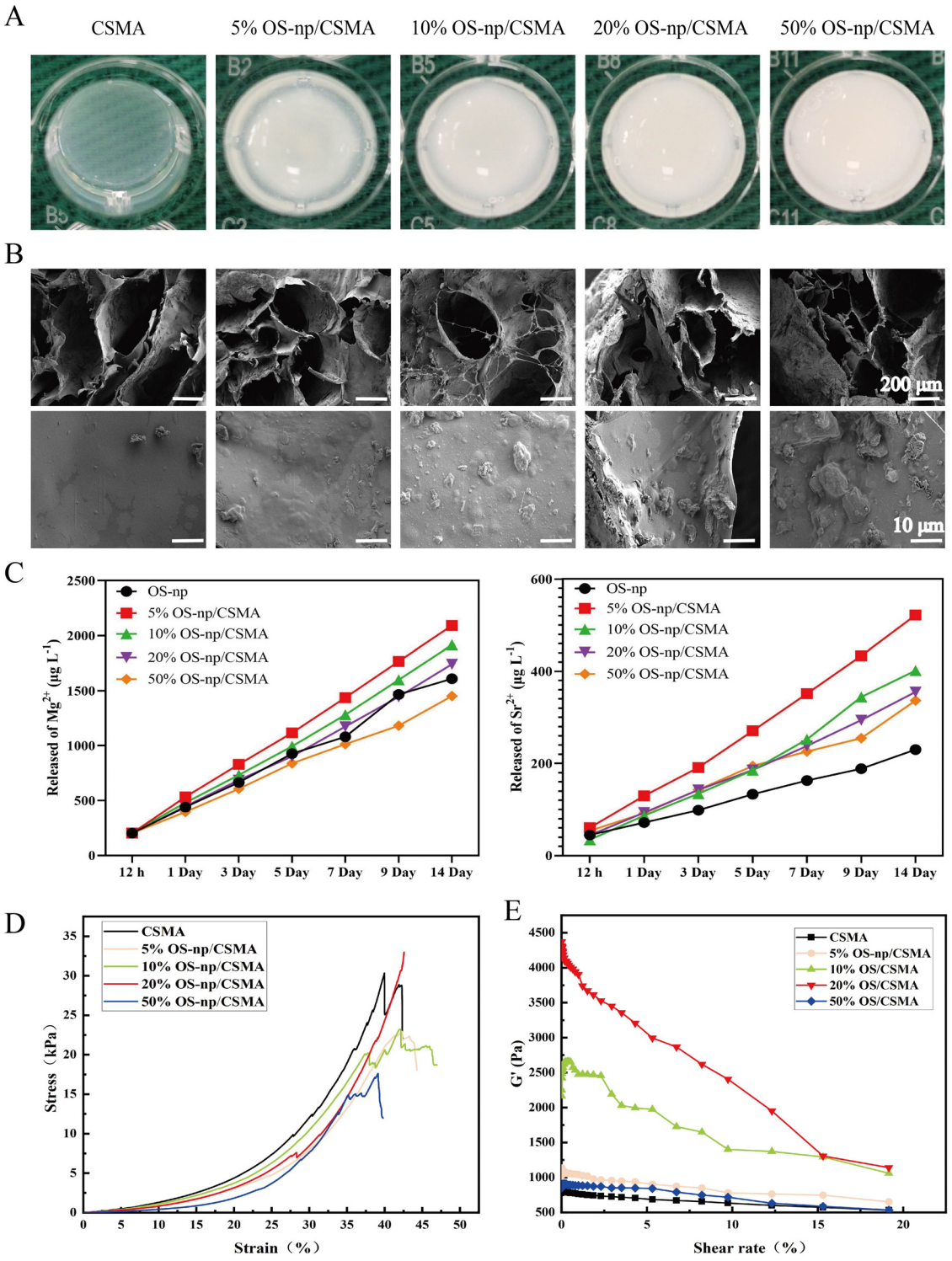

FIG. 3. Preparation and characterization of OS-np/CSMA bone cement. (a) Macroscopic images of CSMA and CSMA with 5%, 10%, 20%, and 50% OS-np. (b) SEM images of different OS-np/CSMA bone cements showing structural morphology at different magnifications. (c) Release concentrations of Mg^{2+} and Sr^{2+} from different OS-np/CSMA bone cement at various times (12 , 1 day, 3 days, 5 days, 7 days, 9 days, and 14 days). (d) Stress–strain curves of different OS-np/CSMA bone cement groups. (e) Relationship between shear rate and viscosity for different OS-np/CSMA bone cement groups.

pore sizes (usually 100–500 μm) and high porosity to facilitate cell infiltration, nutrient exchange, and angiogenesis.[24] SEM scans showed that all OS-np/CSMA groups had good porosity, with pore sizes suitable for cell growth and migration.[25] It could be observed that the surface of CSMA alone was smooth. As OS-np was added, the surface of the hydrogel became rough and particles appeared with increasing OS-np concentration [Fig. 3(b)], indicating the successful synthesis of OS-np/CSMA. Although OS-np alone released Mg^{2+} and Sr^{2+}, their concentrations were relatively low. Interestingly, the addition of CSMA promoted ion release from OS-np and this enhanced release was sustained [Fig. 3(c)]. We hypothesized that the high porosity of the OS-np/CSMA bone cement increases the contact area between OS-np and the liquid, facilitating ion release. Next, the mechanical properties of the bone cement were evaluated. Compression tests showed that the 20% OS-np/CSMA bone cement had the highest mechanical strength, which was higher than that of the CSMA group, and there was no obvious fracture or rupture when compressed to 40% of the original height. In contrast, the other OS-np/CSMA bone cement groups had a lower mechanical strength than the CSMA group alone and exhibited varying degrees of rupture [Fig. 3(d)]. To study the rheological properties of the different OS-np/CSMA hydrogel groups, we performed fixed-frequency amplitude tests to measure the modulus changes with stress and strain [Fig. 3(e)]. It was found that the bone cement of the different OS-np/CSMA groups had a higher storage modulus at different shear rates than that of the CSMA group, indicating that the addition of OS-np can improve the elasticity of CSMA hydrogels, with the 20% OS-np/CSMA group showing the most significant improvement. In summary, the 20% OS-np/CSMA sample exhibited superior mechanical properties. Therefore, unless otherwise specified, the OS/CSMA group mentioned below refers to 20% OS-np/CSMA bone cement. Figure 3 of the supplementary material shows the porosity data for various bone cement groups. The porosity of the standard CSMA was approximately 94.6%, which significantly decreased to 85.7% with 20% OS-np and further to 73.9% with 50% OS-np. These findings demonstrate that increasing the concentration of OS-np results in a gradual reduction in bone cement porosity. As a lower porosity is known to correlate with more stable mechanical properties, the 20% OS-np group exhibited the most suitable balance between porosity and mechanical strength.

C. Assessment of OS-np/CSMA bone cement *in vitro*

Biocompatibility of synthetic materials is important for bone regeneration.[26] We evaluated the biocompatibility of the bone cement using cell viability and CCK-8 assays. Live/dead staining of HUVECs showed that the prepared OS-np/CSMA was non-cytotoxic and exhibited excellent biocompatibility, with only a few red spots observed at 1, 3, and 7 days, indicating the excellent biocompatibility of the OS-np/CSMA bone cement [Fig. 4(a)]. The Rat-BMSCs exhibited the same phenomenon [Fig. 4(b)].

Cell viability and cytotoxicity were evaluated using a CCK-8 assay. HUVECs and Rat-BMSCs were treated with extract solutions from each group for 1, 3, and 7 days. During this period, there was no notable variation in cell viability between the OS-np/CSMA groups with different OS-np concentrations and the control group, confirming that OS-np/CSMA was nontoxic to both cell types and did not affect their normal growth [Fig. 4(c)]. Additionally, H&E staining of the rat viscera at 4 and 8 weeks showed no significant differences between the CSMA, OS-np, OS-np/CSMA, and control groups, with intact tissue structures and no pathological changes [Figs. 4 and 5, supplementary material]. This confirms that OS-np/CSMA has outstanding biocompatibility and is nontoxic to major organs *in vivo*. This meets the basic conditions for bone cement.[27]

D. Evaluation of bone regeneration

Bone marrow mesenchymal stem cells (BMSCs) possess self-renewal and multilineage differentiation capabilities and play a crucial role in bone nonunion repair.[28] Promoting the osteogenic differentiation of BMSCs is advantageous for bone nonunion repair.[29] To assess the osteogenic function of OS-np/CSMA, BMSCs were treated with extract solutions from different groups for 7 days, and immunofluorescence was used to detect the fluorescence expression levels of BMP2 and RUNX2 in BMSCs [Fig. 5(a)]. The fluorescence intensity of BMP2 in the OS-np/CSMA group alone was 2.37 times higher than that in the control group, whereas that of RUNX2 was 1.67 times higher. Moreover, OS-np/CSMA significantly enhanced the osteogenic function in the osteogenic induction medium [Figs. 5(b) and 5(c)].

To evaluate the osteogenic function of OS-np/CSMA, we performed Alizarin Red S (ARS) staining, alkaline phosphatase (ALP) staining, and analyzed bone-related gene expression in BMSCs. Figures 5(d)–5(h) show that compared to the untreated group, both the OS-np and OS-np/CSMA groups exhibited significantly enhanced ARS and ALP staining signals. In contrast, the CSMA group did not show an improvement in ARS and ALP staining signals compared to the control group [Figs. 5(d)–5(h)]. After culturing BMSCs in osteogenic culture medium for 14 days, ARS and ALP staining signals were approximately 2.33-fold and 1.99-fold stronger, respectively, than those in untreated cells. Nonetheless, treatment with OS-np/CSMA extract further enhanced ARS and ALP staining signals, approximately 2.97-fold and 1.49-fold stronger than the osteogenic culture medium group [Figs. 5(d) and 5(e)]. Additionally, both OS-np and OS-np/CSMA groups showed upregulated relative mRNA levels of the osteogenic-related genes *BMP2*, *RUNX2*, and *OCN* compared to the untreated group. The mRNA levels of *BMP2*, *RUNX2*, and *OCN* in the osteogenic culture medium group were significantly higher than those in the control group, and OS-np/CSMA enhanced the osteogenesis-promoting effect of the osteogenic culture medium [Figs. 5(i)–5(k)]. These results indicate that OS-np/CSMA effectively promoted osteogenic differentiation in the presence of OS-np. This can be of great help in the repairing of bone nonunion.

E. Evaluation of angiogenesis

Impaired local blood supply often accompanies bone nonunion, making angiogenesis crucial for the repair process.[30] Scratch and tube formation assays were used to validate the angiogenic capacity of OS-np/CSMA. As shown in Fig. 6(a), the healing of scratches in HUVECs at various time points indicated that the OS-np group exhibited better healing than the control group, with OS-np/CSMA showing an even more significant improvement [Fig. 6(a)]. Remarkably, at 24 h, the unhealed area in the OS-np/CSMA group was only 21.1% of the original area compared to 47.9% in the control group [Fig. 6(b)]. Almost complete healing was observed at 24 h,

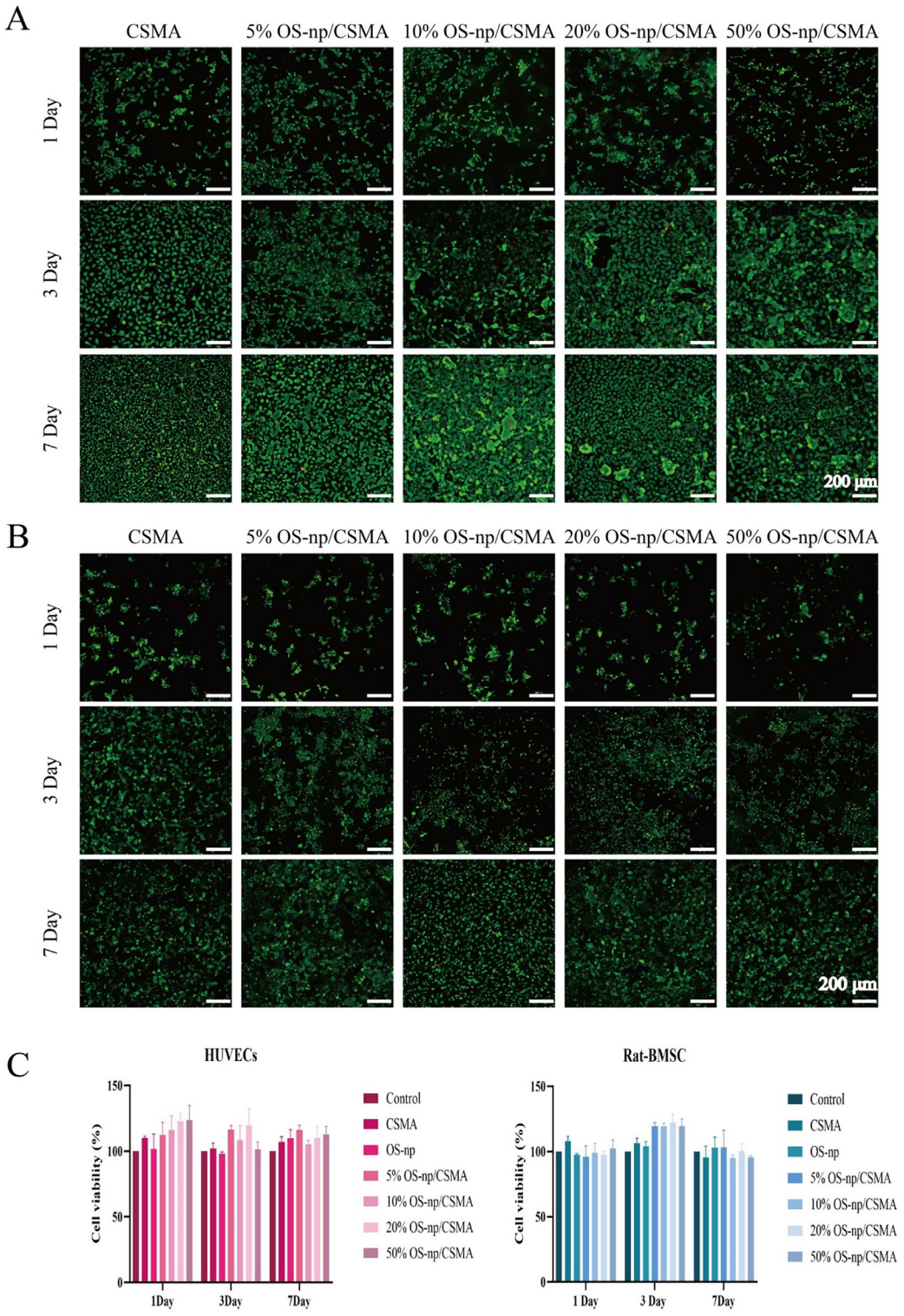

FIG. 4. Assessment of OS-np/CSMA. (a) Live/dead staining fluorescence analysis of HUVECs cultured in different groups of OS-np/CSMA bone cement for 1, 3, and 7 days. (b) Live/dead staining fluorescence analysis of Rat-BMSCs cultured in different groups of OS-np/CSMA for 1, 3, and 7 days. (c) Cell viability analysis of HUVECs and Rat-BMSCs co-cultured with extracts of different groups of OS-np/CSMA for 1, 3, and 7 days.

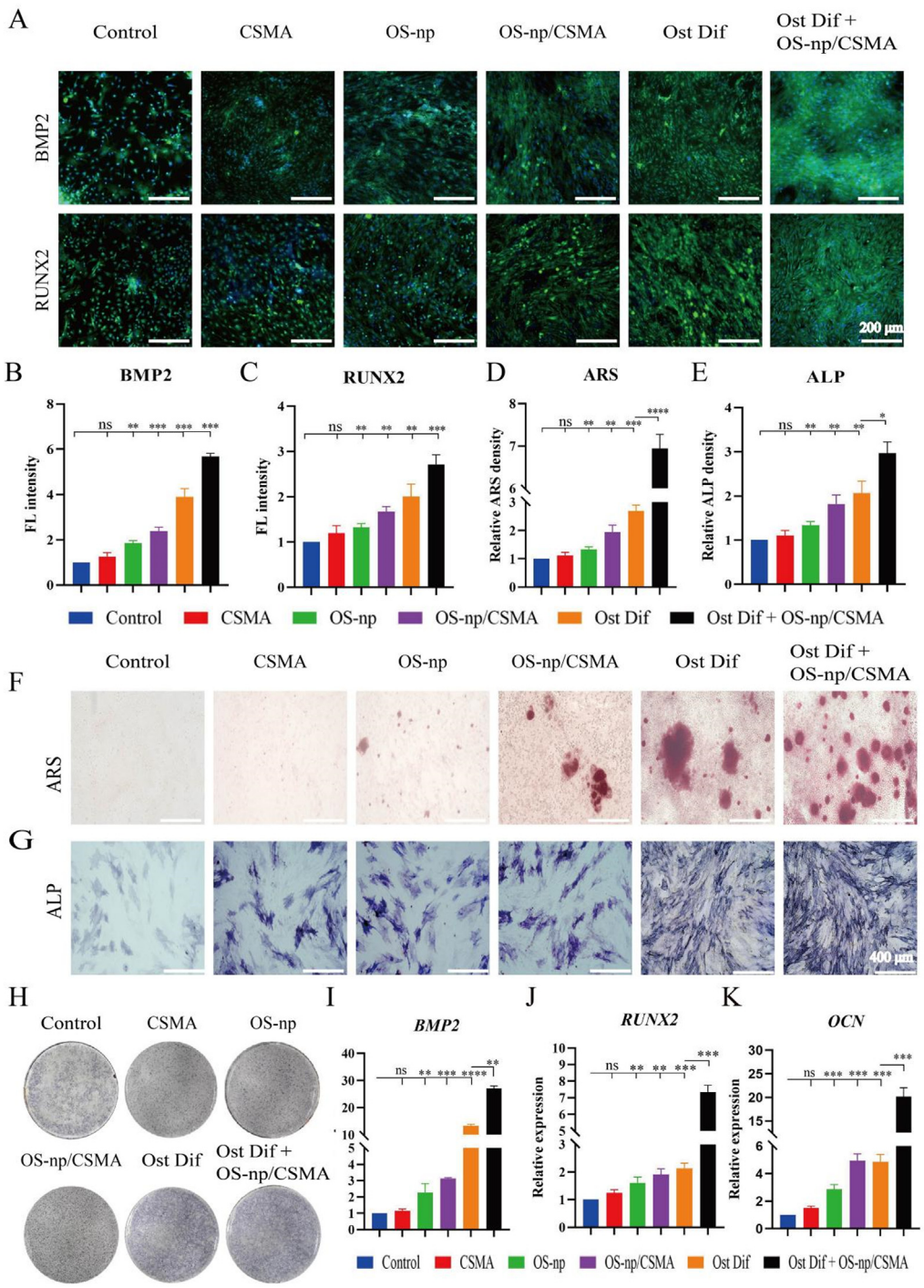

FIG. 5. Osteogenic effectiveness of OS-np/CSMA. (a) Immunofluorescence staining of BMP2 and RUNX2 in Rat-BMSCs co-cultured with CSMA, OS-np, OS-np/CSMA, Ost Dif, Ost Dif+OS-np/CSMA, and normal cell culture medium (control group) for 7 days, (b) quantitative analysis of BMP2, and (c) quantitative analysis of RUNX2. (f) ARS staining images and (d) quantitative analysis of Rat-BMSCs co-cultured for 14 days with CSMA, OS-np, OS-np/CSMA, Ost Dif, Ost Dif+OS-np/CSMA, and normal cell culture medium (control group). (h) ALP staining images in a 12-well plate after 7 days of co-culture. (g) Magnified view at 10× focus. Scale bar = 400 μm. (e) Relative ALP staining density from H. (i) Relative mRNA levels of *BMP2* in different groups. (*BMP2*: Bone Morphogenetic Protein 2). (j) Relative mRNA levels of *RUNX2* in different groups. (*RUNX2*: Runt-related Transcription Factor 2). (k) Relative mRNA levels of *OCN* in different groups. (*OCN*: Osteocalcin) n = 3, $^{*}p < 0.05$, $^{**}p < 0.01$, $^{***}p < 0.001$, $^{****}p < 0.0001$, and "ns" indicated non-significant differences.

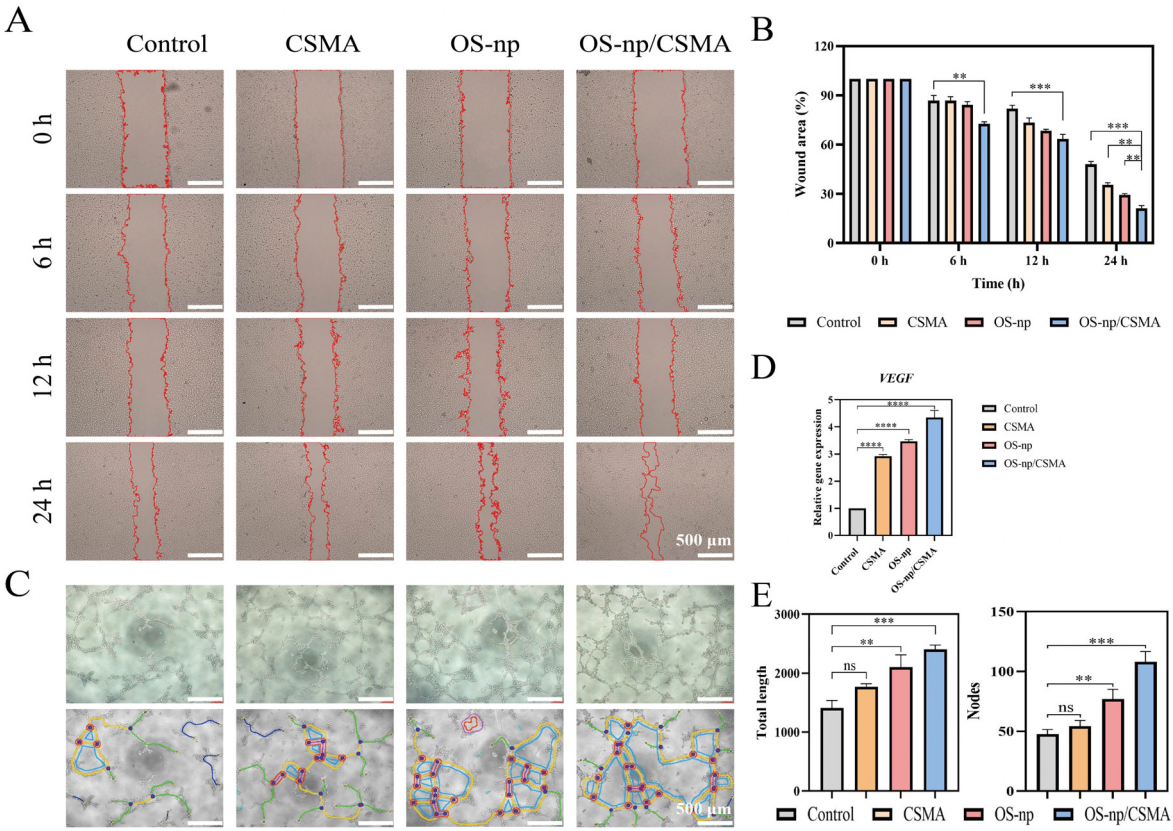

FIG. 6. Angiogenic effectiveness of OS-np/CSMA. (a) Wound healing assay of HUVECs treated with CSMA, OS-np, OS-np/CSMA extracts, and normal culture medium (control group) at various times (0 h, 6 h, 12 h, and 24 h). (b) Quantitative analysis of cell migration distance in the wound healing assay. (c) Tubule formation images of HUVECs co-cultured with CSMA, OS-np, OS-np/CSMA extracts, and normal culture medium (control group) for 4 h. (d) Relative mRNA levels of *VEGF* in HUVECs after co-culture with CSMA, OS-np, OS-np/CSMA extracts, and normal culture medium (control group) for 4 h (*VEGF*: vascular endothelial growth factor). (e) Quantitative analysis of relative tube length and the number of nodes in the tubule formation assay. n = 3, $^{*}p < 0.05$, $^{**}p < 0.01$, $^{***}p < 0.001$, $^{****}p < 0.0001$, and "ns" indicated non-significant differences.

suggesting that OS-np/CSMA significantly enhanced HUVEC migration *in vitro*.

HUVECs were incubated with the extracts of CSMA, OS-np, OS-np/CSMA, or normal cell culture medium (control group) for 6 h, followed by microscopic examination. Compared to the control group, both OS-np and OS-np/CSMA promoted tube formation in HUVECs, with OS-np/CSMA demonstrating more pronounced effects [Fig. 6(c)]. RT-qPCR results showed that the expression level of *VEGF* in the OS-np/CSMA group was 4.3 times higher than that in the control group, demonstrating that OS-np/CSMA significantly enhanced *VEGF* expression [Fig. 6(d)]. *VEGF* is an important genetic marker of angiogenesis and plays a key role in promoting endothelial cell proliferation and migration, enhancing vascular permeability and regulating vessel stability.[31,32] Quantitative results of node and tube lengths showed that compared to the control group, the OS-np/CSMA extract-treated group exhibited 2.27-fold and 1.7-fold increases in the node number and tube length, respectively [Fig. 6(e)]. The primer sequences used for RT-qPCR are shown in Table I. In conclusion, the ability of OS-np/CSMA to promote endothelial cell migration and angiogenesis *in vitro* was validated, suggesting its potential for supporting *in vivo* bone regeneration by enhancing angiogenesis.

F. Promotion of bone regeneration by OS-np/CSMA *in vivo*

OS-np/CSMA demonstrates promising *in vitro* osteogenic properties. Next, we evaluated the repairing effects of OS-np/CSMA in a rat model of tibial nonunion. After implanting OS-np/CSMA into rats for 4 and 8 weeks, the rat tibiae were examined to assess bone regeneration. Figure 7(a) illustrates the gross observation of the tibial nonunion modeling and material filling [Fig. 7(a)].

In vivo x-ray results at 4 weeks post-modeling showed significant nonunion gap healing in the OS-np and OS-np/CSMA treatment groups, with OS-np/CSMA demonstrating the most significant effect compared to the untreated controls, where nonunion gaps were notably larger [Fig. 7(b)]. By week 8, while the control group exhibited increased bone regeneration compared to that at week 4, the rate remained relatively slow. By contrast, the OS-np and OS-np/CSMA groups, particularly the OS-np/CSMA group, showed markedly enhanced bone repair [Fig. 7(b)]. The micro-CT scans [Fig. 7(c)] corroborated these findings.

Statistical analysis based on micro-CT data was used to calculate the bone volume (BV) to tissue volume (TV) ratio of the tibia at weeks 4 and 8. The BV/TV ratio of the regenerated bone in the

TABLE I. The primer sequences of RT-qPCR.

Gene name	Nucleotide sequence (5′-3′)
β-Actin$_{rat}$-RTF	CCT CTA TGC CAA CAC AGT
β-Actin$_{rat}$-RTR	AGC CAC CAA TCC ACA CAG
BMP2$_{rat}$-RTF	CGT CAA GCC AAA CAC AAA CA
BMP2$_{rat}$-RTR	AGT CAT TCC ACC CCA CAT CA
RUNX2$_{rat}$-RTF	CGA AAT GCC TCT GCT GTT AT
RUNX2$_{rat}$-RTR	CGT TAT GGT CAA AGT GAA ACT CT
OCN$_{rat}$-RTF	AAA GCC CAG CGA CTC TGA
OCN$_{rat}$-RTR	CTC CAA GTC CAT TGT TGA GGT
GAPDH$_{human}$-RTF	GATTTGGTCGTATTGGGCG
GAPDH$_{human}$-RTR	CTGGAAGATGGTGATGG
VECF$_{human}$-RTF	TGT GCC CAC TGA GGA GTC
VECF$_{human}$-RTR	CAT TTG TTG TGC TGT AGG AAG

OS-np/CSMA group was higher than that in the other groups at both time points. At 4 weeks, BV/TV ratios were 1.04, 1.32, and 1.52 times higher in CSMA, OS-np, and OS-np/CSMA groups, respectively, compared to the control group [Fig. 7(d)]. At 8 weeks, BV/TV ratios were 1.02, 1.27, and 1.64 times higher in CSMA, OS-np, and OS-np/CSMA groups, respectively, compared to the control group [Fig. 7(d)]. Trabecular thickness (Tb.Th) at 4 and 8 weeks showed the same trend. At 4 weeks, the Tb.Th ratios of the CSMA, OS-np, and OS-np/CSMA groups were 1.04, 1.36, and 1.68 times higher than those of the control group. At 8 weeks, the Tb.Th ratios of the CSMA, OS-np, and OS-np/CSMA groups were 1.03, 1.42, and 1.58 times higher than the control group, respectively [Fig. 7(e)]. Histological staining with hematoxylin and eosin (H&E) and Masson's trichrome was performed on the tibial defect sites 4 and 8 weeks post-implantation to evaluate tissue regeneration.[33] In the control group, the defect site was predominantly composed of fibrous connective tissue. The CSMA group primarily exhibited fibrous connective tissue with negligible new bone formation. Notably, the OS-np group showed new bone and connective tissue within the defect area. The OS-np/CSMA group demonstrated significant bone regeneration with nearly complete resolution of the bone defect by 8 weeks, which was replaced by robust new bone tissue. These results highlight the enhanced regenerative capacity of the OS-np/CSMA group, which exhibited accelerated bone repair compared with the other experimental groups [Figs. 7(f) and 7(g)].

G. Immunohistochemical staining analysis

To identify the osteogenic effects of OS-np/CSMA *in vivo*, immunohistochemical staining for BMP2 (bone marker) and RUNX2 (bone marker) was performed in different groups. The results at 4 weeks showed that the BMP2 content in the OS-np/CSMA group was significantly higher than that in the control group [Fig. 8(a)], and this difference was even more pronounced at 8 weeks [Fig. 8(d)]. RUNX2 results were consistent with those for BMP2 [Figs. 8(b) and 8(e)]. Quantification of BMP2 at 4 weeks showed that the OS-np/CSMA, OS-np, and CSMA groups were 3.65, 1.85, and 1.03 times higher than the control group, respectively [Fig. 8(g)], and at 8 weeks, the BMP2 quantification showed that the OS-np/CSMA, OS-np, and CSMA groups were 5.47, 3.68, and 1.07 times higher than the control group, respectively [Fig. 8(j)]. Quantification of RUNX2 at 4 weeks showed that the OS-np/CSMA, OS-np, and CSMA groups were 3.87, 2.0, and 1.08 times higher than the control group, respectively [Fig. 8(h)]. At 8 weeks, RUNX2 quantification showed that the OS-np/CSMA, OS-np, and CSMA groups were 4.38, 2.10, and 1.09 times higher than the control group, respectively [Fig. 8(k)]. Additionally, *in vitro* scratch and angiogenesis assays demonstrated that OS-np/CSMA promoted vascular formation, and *in vivo* immunohistochemical staining for VEGF indicated that OS-np/CSMA promoted angiogenesis [Figs. 8(c) and 8(f)]. Quantification of VEGF at 4 weeks showed that the OS-np/CSMA, OS-np, and CSMA groups were 4.11, 3.15, and 1.10 times higher than the control group, respectively [Fig. 8(i)]; at 8 weeks, VEGF quantification showed that the OS-np/CSMA, OS-np, and CSMA groups were 3.54, 2.12, and 1.15 times higher than the control group, respectively [Fig. 8(l)]. These findings suggest that OS-np/CSMA effectively promotes osteogenesis and angiogenesis, providing the necessary nutritional support for bone repair, thereby laying a solid foundation for the regeneration and repair of bone defects, and enhancing bone regeneration and repair in nonunion environments.

III. CONCLUSION

In this study, we developed an injectable photosensitive bone cement that combined CSMA and OS-np to promote the repair of nonunion fractures. The results indicate that OS-np/CSMA bone cement has the following advantages: (a) Excellent Porous Structure: The OS-np/CSMA bone cement exhibits suitable porosity, promotes cell growth, and enhances material hardness. (b) Reinforced Structure: Incorporating OS-np into CSMA resulted in a reinforced concrete-like structure, further improving the hardness of the material. (c) Regulation of the nonunion bone microenvironment: OS/CSMA promotes vascular formation, providing nutrients to the nonunion bone microenvironment. It also supplies essential calcium and various other osteogenesis-promoting ions (Ca^{2+}, Mg^{2+}, Sr^{2+}, and Si^{4+}), thereby facilitating bone formation. In conclusion, OS-np/CSMA bone cement not only exhibits excellent biocompatibility and mechanical properties but also effectively provides a treatment strategy for nonunions by promoting vascularization and the migration and differentiation of osteoblasts. Bone cement shows promise as a clinical treatment method for addressing the challenging issue of complex nonunion repairs.

IV. METHODS

A. Materials

Dulbecco's modified eagle medium (DMEM) cell culture medium and fetal bovine serum (FBS) were purchased from Gibco (UK). Cell lines including bone marrow mesenchymal stem cells (BMSC) and human umbilical vein endothelial cells (HUVECs) were cultured with a complete medium (DMEM cell culture medium with 10% FBS) in an incubator (37 °C, 5% CO_2).

B. Preparation of CSMA

CSMA was synthesized through a one-step N-acetylation reaction between high-density CS and MA. The process was as follows: CS was dissolved in 1% (w/v) acetic acid solution and stirred at 60 °C to obtain a 1% (w/v) CS solution. MA was then added to the CS solution, and the mixture was stirred at 60 °C for 12 h to synthesize CSMA. The solution was neutralized with 1 wt. % saturated sodium bicarbonate solution. The product was dialyzed in ddH_2O for 48 h to remove

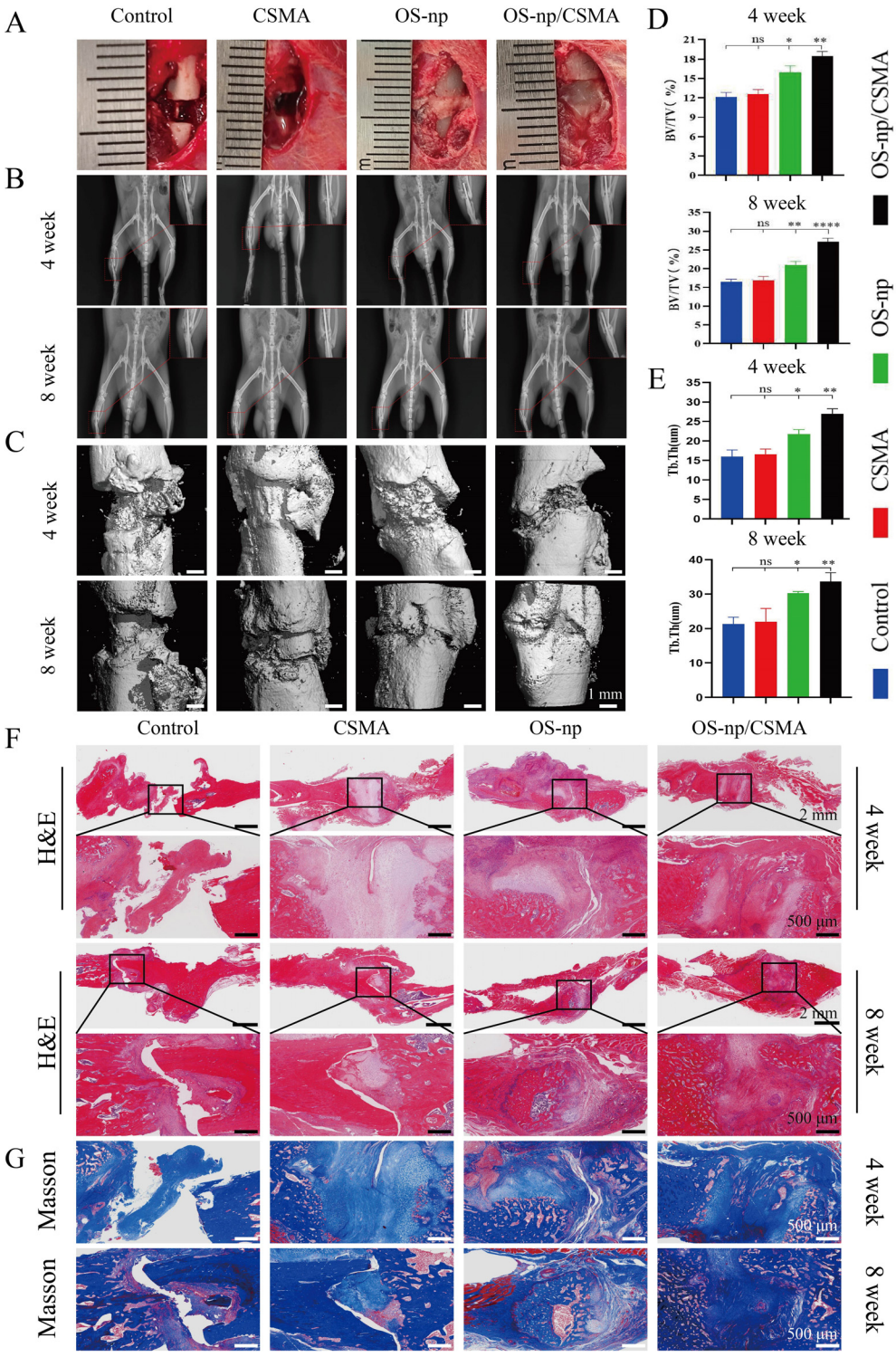

FIG. 7. Evaluation of angiogenesis promotion by OS-np/CSMA *in vivo*. (a) Surgical method of nonunion in rat tibia. (b) x-ray images of the CSMA, OS-np, OS-np/CSMA, and control groups at 4 and 8 weeks. (c) Micro-CT images of the CSMA, OS-np, OS-np/CSMA, and control groups at 4 and 8 weeks. (d) Quantification of regenerated bone tissue BV/TV at 4 and 8 weeks. (E) Quantification of Tb.Th at 4 and 8 weeks. $n = 3$, $^{*}p < 0.05$, $^{**}p < 0.01$, $^{***}p < 0.001$, $^{****}p < 0.0001$, and "ns" indicated non-significant differences. (F) H&E staining images of the tissue at 4 and 8 weeks post-operation. (G) Masson's trichrome staining images of the tissue at 4 and 8 weeks post-operation.

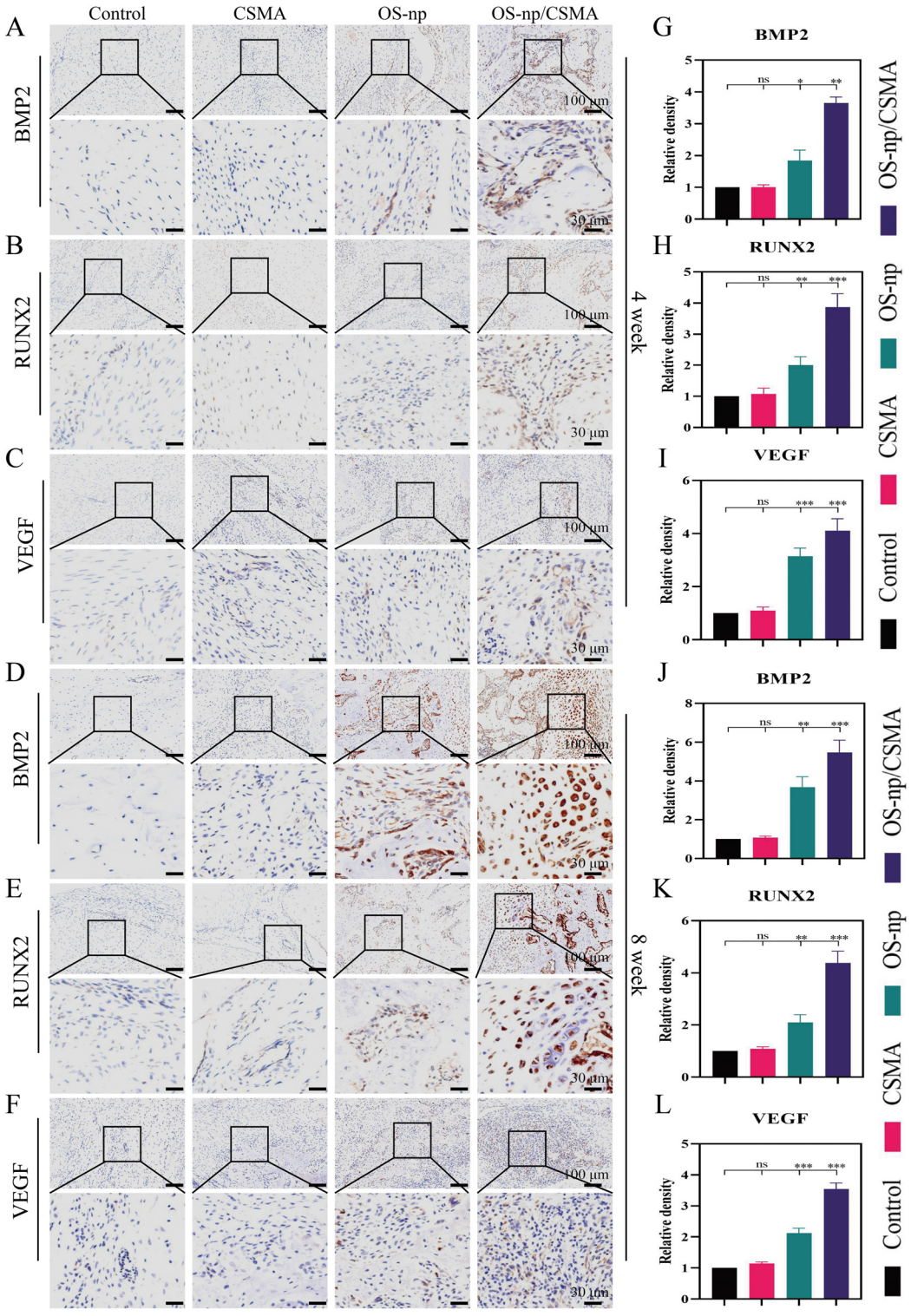

FIG. 8. Immunohistochemical analysis. (a)–(c) BMP2, RUNX2, and VEGF immunohistochemical staining at 4 weeks. (d)–(f) BMP2, RUNX2, and VEGF immunohistochemical staining at 8 weeks. (g)–(i) Quantitative analysis of BMP2, RUNX2, and VEGF immunohistochemical staining at 4 weeks. (j)–(l) Quantitative analysis of BMP2, RUNX2, and VEGF immunohistochemical staining at 8 weeks. $n = 3$, $^{*}p < 0.05$, $^{**}p < 0.01$, $^{***}p < 0.001$, $^{****}p < 0.0001$, and "ns" indicated non-significant differences.

unreacted reagents. Finally, the material was lyophilized and stored at 4 °C for later use.

C. Preparation and characterization of OS-np

Separate approximately 1000 g of fresh oysters were separated from their shells. The oyster shells were thoroughly rinsed with distilled water and allowed to air-dry. An electric grinder was used to pulverize the shells into powder. The powder was sieved through a 300-mesh screen to ensure that the particle size was below 300 mesh. The powder was soaked in chloroform solution and stirred for 24 h. After washing with ddH_2O, the powder was dried in a hot-air oven. Fourier transform infrared (FTIR) analysis of the oyster shell (OS) was performed using a Bruker INVENIO from Germany, and EDS was performed using an Oxford Instruments AZtecLive Ultim Max 100 to determine its major elemental composition. Finally, XRD analysis was conducted using a Rigaku SmartLab SE instrument from Japan.

D. Preparation of OS-np/CSMA bone cement

Initially, 50 mg OS-np was dissolved in 1 ml double-distilled water to prepare a 50 mg/ml OS-np aqueous solution. Subsequently, varying volumes (0.05, 0.1, 0.2, and 0.5 ml) of the OS-np aqueous solution were added to CSMA, adjusted to 1 ml total volume with CSMA, to achieve concentrations of 5%, 10%, 20%, and 50% OS-np in the bone cement, respectively.

E. Compression test

The compressive strength of OS-np/CSMA bone cement was measured using a mechanical testing machine (Shimadzu AGS-X-50N, Japan) at a compression rate of 1 mm/min to obtain the stress–strain curve of the material.

F. Rheological test

The dynamic viscoelasticities of the hydrogel were measured with a Haake Mars60 rheometer from Germany. The test frequency was fixed at 1 Hz to observe the variation in the hydrogel modulus with the shear rate, delineating its linear viscoelastic range.

G. *In vitro* release of $Mg2^+$ and $Sr2^+$ from OS-np and OS-np/CSMA bone cement

3.5 mg of OS-np and bone cement containing various concentrations of OS-np/CSMA with 3.5 mg of OS-np were each immersed in 10 ml of pure water (pH = 7.0). At predetermined time points (0 h, 12 h, 1 day, 3 days, 5 days, 7 days, 9 days, and 14 days), 1 ml of the solution was extracted from each sample. The concentrations of Mg^{2+} and Sr^{2+} were quantitatively determined using ICP-OES (Agilent 720ES, USA). After each sampling, the volume of liquid in each container was replenished to 10 ml to maintain consistent conditions for measuring cumulative release.

H. Living/dead cell double staining

The HUVECs and BMSCs were separately mixed into the prepared OS-np/CSMA bone cement containing different concentrations of OS-np at a density of 5×10^6 cells/ml. The cell-loaded hydrogels were evenly seeded into six-well plates, with CSMA alone as the control group. Each group was supplemented with 3 ml of complete culture medium and tested at 1, 3, and 7 days. After removing the culture medium, the samples were immersed in pre-prepared Calcein-AM/PI solution and incubated at 37 °C for 15 min. Following incubation, cell images from different groups were captured using a fluorescence microscope (Leica SP5, Leica Camera AG, Germany).

I. CCK-8 assay

OS-np/CSMA bone cements containing different concentrations of OS-np were immersed in 10 ml of high-glucose/low-glucose DMEM for 24 h to prepare the extracts. HUVECs/BMSCs were seeded into 96-well plates at a density of 3000 cells/well and divided into six groups: control, CSMA, 5% OS-np/CSMA, 10% OS-np/CSMA, 20% OS-np/CSMA, and 50% OS-np/CSMA. Cells were co-cultured with the extracts for 1, 3, or 7 days. A solution containing 10% CCK-8 was added to each well, and the plates were incubated at 37 °C for 1 h. Absorbance was measured using a SpectraMAX iD3 microplate reader. Each group was repeated five times to ensure statistical reliability and to calculate cell viability.

J. Bone regeneration test *in vitro*

The BMSCs were seeded in a 12-well plate at a density of 5×10^4 cells/well. Cells were co-cultured with the CSMA extract, OS-np extract, OS-np/CSMA extract, osteogenic culture medium, or osteogenic culture medium with the OS-np/CSMA extract. A complete medium without any material was used as the control group. ALP staining was performed after 7 days of co-culture, and ARS was performed after 14 days. At predetermined times, the medium was discarded and the cells were fixed with 4% paraformaldehyde for 10 min. After washing with PBS, the cells were stained with alkaline phosphatase/Alizarin Red staining solution for 30 min. The staining solution was removed, and the cells were washed twice with PBS. The 12-well plates were then observed and photographed under a microscope.

K. Tube formation analysis

First, 50 μl of matrix gel was added to a 96-well plate and incubated at 37 °C for 40 min to allow the matrix gel to solidify without forming bubbles. The HUVECs were seeded at a density of 3×10^4 cells/well in a 96-well plate. Cultured HUVECs were divided into four groups, each receiving different treatments: CSMA extract, OS-np extract, or OS-np/CSMA extract complete medium without materials was used as the control group. The cells were incubated at 37 °C for 6 h to allow tube formation and then imaged using a microscope. Tube length and node number in each treatment group were analyzed using Image J software.

L. Cell migration *in vitro*

HUVECs were seeded into a 12-well plate at approximately 2.5×10^5 cells per well. A straight scratch was created along the cell monolayer using a pipette tip, and the cells were gently washed with PBS to remove detached cells. Then, the cells were treated with serum-free medium containing CSMA, OS-np, and OS-np/CSMA extracts. A serum-free medium without any extract was used as a control. To monitor cell migration, photographs of the same area were captured at 0, 6, 12, and 24 h.

M. RT-qPCR

BMSCs and HUVECs in culture dishes were extracted using TRIzol reagent (Solarbio, Beijing, China). RNA concentration was measured at 260 nm using a microplate reader (Thermo Scientific, USA). Reverse transcribe the RNA into cDNA. RT-qPCR was conducted using the SYBR Green Real-time PCR Master Mix on a real-time PCR system (TOYOBO, Japan), following the manufacturer's protocol: RT-qPCR procedure: 95 °C for 3 min, followed by 40 cycles of 95 °C for 5 s, 60 °C for 30 s, and melt for 15 s. Data were analyzed using the formula: $R = 2^{-[\Delta Ct\ sample - \Delta Ct\ control]}$, where R represents relative expression levels, ΔCt indicates the difference between the Ct values of the target gene and GAPDH in the experimental sample, and ΔCt control represents the difference between the Ct values of the target gene and GAPDH in the control sample. The experiment was performed in triplicate using independent experimental samples.

N. *In vivo* animal study

The experiment used male specific pathogen-free (SPF) rats, weighing approximately 300 g, provided by Jiangsu Jicui Yaokang Biotechnology Co., Ltd. The rats were randomly divided into four groups: control, CSMA, OS-np, and OS-np/CSMA, with $n \geq 6$ per group. Surgery was performed after anesthetizing the rats with 3% pentobarbital sodium. A 10 mm lateral skin incision was made, and the muscles were bluntly dissected to expose the right tibia. A transverse osteotomy was performed using an electric saw. A 3 mm section of the tibia was removed at the middle distal third of the tibia, and a 0.8 mm diameter Kirschner wire was inserted into the tibial shaft to create a nonunion model. The defect was filled with the CSMA hydrogel, OS-np/CSMA composite hydrogel, and OS-np bone cement. The hydrogels were photo-cured with 405 nm UV light for 30 s, while the control group received no filling. After fixation, the site was disinfected and sutured, and penicillin was administered for three days post-surgery to prevent infection.

O. X-ray and micro-CT

Three days post-surgery, the rats were anesthetized for x-ray scanning to observe the stability of the bone nonunion defect area. Bone regeneration was assessed at 4 and 8 weeks post-implantation. At 4 and 8 weeks after implantation, the tibiae were extracted and scanned using a micro-CT (Scanco, Switzerland) to observe bone regeneration.

P. Histological evaluation and immunohistochemical staining

The tibiae were fixed in 4% paraformaldehyde for at least 24 h, followed by decalcification in 10% EDTA solution for approximately 1 month. Tissue samples were embedded in paraffin and sectioned into 3 μm thick cross sections at the center of the defect. Staining was performed using H&E and Masson's trichrome staining. Immunohistochemical staining was performed for Bone Morphogenetic Protein 2 (BMP2), Runt-related Transcription Factor 2 (RUNX2), and osteocalcin (OCN) to evaluate bone morphology and protein expression.

Q. Statistical analysis

Data were collected in three or five sets and reported as mean ± standard deviation. The scratch area, angiogenesis data, and quantitative fluorescence data were analyzed using Image J, while all other data were evaluated using GraphPad Prism. Statistical significance was determined as $^{*}p < 0.05$, $^{**}p < 0.01$, $^{***}p < 0.001$, $^{****}p < 0.0001$, and "ns" indicated non-significant differences.

SUPPLEMENTARY MATERIAL

See the supplementary material for five additional supplementary material referenced in the text, including additional information about the injectability of OS-np/CSMA (supplementary material Fig. 1), the FT-IR of OS-np (supplementary material Fig. 2), the porosity of different bone cement groups (supplementary material Fig. 3), H&E staining of major organs (heart, liver, spleen, lung, and kidney) from rats treated with CSMA, OS-np, OS-np/CSMA, and control group at 4 weeks (supplementary material Fig. 4), and H&E staining of major organs (heart, liver, spleen, lung, and kidney) from rats treated with CSMA, OS-np, OS-np/CSMA, and control group at 8 weeks (supplementary material Fig. 5).

ACKNOWLEDGMENTS

This work is financially supported by the Key Research and Development Program of Henan Province (No. 221111310100); the Henan Provincial Science and Technology Research and Development Joint Fund (Industrial) (No. 235101610001); the Open Research Fund of the Tissue Engineering and Regenerative Clinical Medical Center of Xinxiang Medical University (Nos. 2022YFYKFKT01, 2022KFKTZD03, 2022YFYKFKT05, and 2022YFYKFKT07); the Key Research and Development and Promotion Special (Science and Technology) Project of Henan Province (No. 242102310321); the Open Project Program of the Third Affiliated Hospital of Xinxiang Medical University (No. KFKTZD202105); and the Henan Province Key Scientific Research Project Plan for Higher Education Institutions (No. 25A430023).

AUTHOR DECLARATIONS

Conflict of Interest

The authors have no conflicts to disclose.

Ethics Approval

Ethics approval for experiments reported in the submitted manuscript on animal or human subjects was granted. All experimental procedures were conducted in accordance with institutional guidelines for the care and use of laboratory animals and protocols (ID No.: LL-202401260001), which were approved by the Animal Care and Use Committee of Shanghai Ninth People's Hospital.

Author Contributions

Mengnan Wen and Xueqiang Guo contributed equally to this work.

Mengnan Wen: Data curation (lead); Methodology (lead); Writing – original draft (lead). **Xueqiang Guo:** Data curation (equal); Formal analysis (lead); Supervision (equal). **Yan Gong:** Data curation

(supporting); Software (lead). **Fei Xue:** Data curation (equal); Investigation (equal). **Zhenlin Fan:** Project administration (lead); Supervision (equal). **Zhanting Kang:** Methodology (equal); Software (supporting). **Jixiang Li:** Software (equal); Validation (equal). **Lei Wang:** Funding acquisition (equal); Project administration (equal). **Xiansong Wang:** Conceptualization (lead); Project administration (lead); Writing – review & editing (lead). **Wenjie Ren:** Conceptualization (equal); Funding acquisition (lead); Writing – review & editing (equal).

DATA AVAILABILITY

The data that support the findings of this study are available within the article and its supplementary material.

REFERENCES

[1]B. Wildemann, A. Ignatius, F. Leung, L. A. Taitsman, R. M. Smith, R. Pesántez, M. J. Stoddart, R. G. Richards, and J. B. Jupiter, "Non-union bone fractures," Nat. Rev. Dis. Primers **7**(1), 57 (2021).

[2]P. Andrzejowski and P. V. Giannoudis, "The 'diamond concept' for long bone non-union management," J. Orthop. Traumatol. **20**(1), 21 (2019).

[3]G. F. Rogers and A. K. Greene, "Autogenous bone graft: Basic science and clinical implications," J. Craniofacial Surg. **23**(1), 323–327 (2012).

[4]Z. Stopa, M. Siewert-Gutowska, K. Abed, D. Szubińska-Lelonkiewicz, A. Kamiński, and P. Fiedor, "Evaluation of the safety and clinical efficacy of allogeneic bone grafts in the reconstruction of the maxilla and mandible," Transplant. Proc. **50**(7), 2199–2201 (2018).

[5]J. Yang, X. Zhang, W. Liang, G. Chen, Y. Ma, Y. Zhou, R. Fen, and K. Jiang, "Efficacy of adjuvant treatment for fracture nonunion/delayed union: A network meta-analysis of randomized controlled trials," BMC Musculoskelet. Disord. **23**(1), 481 (2022).

[6]S. S. Phull, A. R. Yazdi, M. Ghert, and M. R. Towler, "Bone cement as a local chemotherapeutic drug delivery carrier in orthopedic oncology: A review," J. Bone Oncol. **26**, 100345 (2021).

[7]S. Mistry, R. Roy, A. K. Jha, N. Pandit, S. Das, S. Burman, and M. Joy, "Treatment of long bone infection by a biodegradable bone cement releasing antibiotics in human," J. Controlled Release **346**, 180–192 (2022).

[8]K. Hurle, J. M. Oliveira, R. L. Reis, S. Pina, and F. Goetz-Neunhoeffer, "Ion-doped brushite cements for bone regeneration," Acta Biomater. **123**, 51–71 (2021).

[9]Y. Tang, L. Chen, Z. Wu, K. Zhao, and Q. Tan, "Fabrication of injectable and expandable PMMA/PAAS f bone cements," Compos. Sci. Technol. **146**, 203–209 (2017).

[10]P. Wang, Y. Gong, G. Zhou, W. Ren, and X. Wang, "Biodegradable implants for internal fixation of fractures and accelerated bone regeneration," ACS Omega **8**, 27920−−27931 (2023).

[11]S. I. Ahmad, R. Ahmad, Mohd., S. Khan, R. Kant, S. Shahid, L. Gautam, G. M. Hasan, and Md. I. Hassan, "Chitin and its derivatives: Structural properties and biomedical applications," Int. J. Biol. Macromol. **164**, 526–539 (2020).

[12]L. Moradi, L. Witek, V. Vivekanand Nayak, A. Cabrera Pereira, E. Kim, J. Good, and C. Liu, "Injectable hydrogel for sustained delivery of progranulin derivative Atsttrin in treating diabetic fracture healing," Biomaterials **301**, 122289 (2023).

[13]Y. Xu, Z. Deng, Y. Chen, F. F. Wu, C. Huang, and Y. Hu, "Preparation and characterization of mussel-inspired hydrogels based on methacrylated catechol-chitosan and dopamine methacrylamide," Int. J. Biol. Macromol. **229**, 443–451 (2023).

[14]P. Dai, X. Ge, C. Sun, H. Jiang, W. Zuo, P. Wu, C. Liu, S. Deng, J. Yang, J. Dai, and Y. Ju, "A novel methacryloyl chitosan hydrogel microneedles patch with sustainable drug release property for effective treatment of psoriasis," Macromol. Biosci. **23**(12), 2300194 (2023).

[15]J. Wang, L. Xie, X. Wang, W. Zheng, H. Chen, L. Cai, and L. Chen, "The effects of oyster shell/alpha-calcium sulfate hemihydrate/platelet-rich plasma/bone mesenchymal stem cells bioengineering scaffold on rat critical-sized calvarial defects," J. Mater. Sci.: Mater. Med. **31**(11), 96 (2020).

[16]X. Feng, S. Jiang, F. Zhang, R. Wang, Y. Zhao, and M. Zeng, "Shell water-soluble matrix protein from oyster shells promoted proliferation, differentiation and mineralization of osteoblasts *in vitro* and *vivo*," Int. J. Biol. Macromol. **201**, 288–297 (2022).

[17]R. LogithKumar, A. KeshavNarayan, S. Dhivya, A. Chawla, S. Saravanan, and N. Selvamurugan, "A review of chitosan and its derivatives in bone tissue engineering," Carbohydr. Polym. **151**, 172–188 (2016).

[18]T. Qi, J. Weng, F. Yu, W. Zhang, G. Li, H. Qin, Z. Tan, and H. Zeng, "Insights into the role of magnesium ions in affecting osteogenic differentiation of mesenchymal stem cells," Biol. Trace Elem. Res. **199**(2), 559–567 (2021).

[19]T. Chen, H. Huang, J. Cao, Y. Xin, W. Luo, and N. Ao, "Preparation and characterization of alginate/HACC/oyster shell powder biocomposite scaffolds for potential bone tissue engineering applications," RSC Adv. **6**(42), 35577–35588 (2016).

[20]S. J. Waddell, M. C. De Andrés, P. M. Tsimbouri, E. V. Alakpa, M. Cusack, M. J. Dalby, and R. O. Oreffo, "Biomimetic oyster shell–replicated topography alters the behaviour of human skeletal stem cells," J. Tissue Eng. **9**, 1–13 (2018).

[21]Y. Shen, S. Yang, J. Liu, H. Xu, Z. Shi, Z. Lin, X. Ying, P. Guo, T. Lin, S. Yan, Q. Huang, and L. Peng, "Engineering scaffolds integrated with calcium sulfate and oyster shell for enhanced bone tissue regeneration," ACS Appl. Mater. Interfaces **6**(15), 12177–12188 (2014).

[22]D. Zhang, J. Liu, Q. Chen, W. Jiang, Y. Wang, J. Xie, K. Ma, C. Shi, H. Zhang, M. Chen, J. Wan, P. Ma, J. Zou, W. Zhang, F. Zhou, and R. Liu, "A sandcastle worm-inspired strategy to functionalize wet hydrogels," Nat. Commun. **12**(1), 6331 (2021).

[23]Y.-K. Lee, S. K. Jung, Y. H. Chang, and H.-S. Kwak, "Highly bioavailable nano-calcium from oyster shell for preventing osteoporosis in rats," Int. J. Food Sci. Nutr. **68**(8), 931–940 (2017).

[24]F. S. L. Bobbert and A. A. Zadpoor, "Effects of bone substitute architecture and surface properties on cell response, angiogenesis, and structure of new bone," J. Mater. Chem. B **5**(31), 6175–6192 (2017).

[25]Y. Han, M. Lian, Q. Wu, Z. Qiao, B. Sun, and K. Dai, "Effect of pore size on cell behavior using melt electrowritten scaffolds," Front. Bioeng. Biotechnol. **9**, 629270 (2021).

[26]Y. Gong, Y. Gan, P. Wang, C. Gong, B. Han, P. Li, E. Liu, Z. Yu, L. Sheng, and X. Wang, "Injectable foam-like scaffolds release glucose oxidase-integrated metal–organic framework hybrids for diabetic bone defects," Appl. Mater. Today **38**, 102190 (2024).

[27]W. Hou, J. Liu, W. Wei, Y. Zhao, X. Wu, and H. Dai, "All-in-one strategy to develop a near-infrared triggered multifunctional bioactive magnesium phosphate bone cement for bone repair," Acta Biomater. **182**, 111–125 (2024).

[28]B. Cai, D. Lin, Y. Li, L. Wang, J. Xie, T. Dai, F. Liu, M. Tang, L. Tian, Y. Yuan, L. Kong, and S. G. F. Shen, "N2-polarized neutrophils guide bone mesenchymal stem cell recruitment and initiate bone regeneration: A missing piece of the bone regeneration puzzle," Adv. Sci. **8**(19), 2100584 (2021).

[29]J. S. Park, S. W. Yi, H. J. Kim, S. M. Kim, and K.-H. Park, "Regulation of cell signaling factors using PLGA nanoparticles coated/loaded with genes and proteins for osteogenesis of human mesenchymal stem cells," ACS Appl. Mater. Interfaces **8**(44), 30387–30397 (2016).

[30]X. Zhou, Y. Qian, L. Chen, T. Li, X. Sun, X. Ma, J. Wang, and C. He, "Flowerbed-inspired biomimetic scaffold with rapid internal tissue infiltration and vascularization capacity for bone repair," ACS Nano **17**(5), 5140–5156 (2023).

[31]Z. Li, Z. Wang, J. Wei, Y. Zhao, and W. Wu, "Angiogenic potential of human bone marrow-derived mesenchymal stem cells in chondrocyte brick-enriched constructs promoted stable regeneration of craniofacial cartilage," Stem Cells Transl. Med. **6**, 601–612 (2017).

[32]X. Fan, Y. Teng, Z. Ye, Y. Zhou, and W. Tan, "Gap junction-mediated MiR-200b on osteogenesis and angiogenesis in coculture between MSCs and HUVECs," J. Cell Sci. **131**(13), jcs216135 (2023).

[33]M. Pei, P. Li, X. Guo, M. Wen, Y. Gong, P. Wang, Z. Fan, L. Wang, X. Wang, and W. Ren, "Sustained release of hydrogen and magnesium ions mediated by a foamed gelatin-methacryloyl hydrogel for the repair of bone defects in diabetes," ACS Biomater. Sci. Eng. **10**(7), 4411–4424 (2024).